Chemical Engineering & Processing: Process Intensification 173 (2022) 108806

Contents lists available at ScienceDirect

Chemical Engineering and Processing - Process Intensification

journal homepage: www.elsevier.com/locate/cep

Determination and optimisation of Resonant Acoustic Mixing (RAM) efficiency in Polymer Bonded eXplosive (PBX) processing

A.J. Claydon[1], A.N. Patil[2], S. Gaulter, G. Kister *, P.P. Gill[3]

Cranfield University, Defence Academy of the United Kingdom, Shrivenham, SN6 8LA, United Kingdom

ARTICLE INFO

Keywords:
Resonant Acoustic Mixing
Polymer Bonded eXplosive
Efficiency
LabRAM

ABSTRACT

An investigation into how the efficiency (time and energy required for homogeneity) of Resonant Acoustic Mixing (RAM) can be determined and optimised was undertaken. An idealised Polymer Bonded eXplosive (PBX) simulant based on glass microbeads (28.3 μm D50, 62% v/v in binder and plasticiser) was used for mixing. Mixing evolution was monitored using machine output data, whereby the mixer 'intensity' (related to power draw) was plotted against time. Experiments were undertaken with three acceleration settings, three mixer units, and three vessel materials of low, medium, and high surface free energy. Different stages of the mixer 'intensity' profiles were found to correspond to discrete stages of mixing, as well as further rheological changes due to continued frictional heating, thus viscosity reduction, beyond homogeneity being achieved. Time to mixing completion was found to be repeatable within a standard deviation of ±10%, strongly dependent on acceleration setting, and additionally dependent on vessel material, though additional data is required to confirm this. A significant difference in mixing time was observed between different LabRAM units. Partial vacuum application without degassing was beneficial for mixing. Finally, a paradigm linking the 'movement modes' of mixing was constructed, based on literature observations and the experimental results.

1. Introduction

High shear mixing of loaded suspensions is required in industries such as food, cosmetics, and energetic materials, where the requirement to mix high viscosity pastes precludes the use of turbulent mixing techniques such as those involving impeller blades. Typically, the mixing mechanism will instead involve laminar flow, and rely on shearing, kneading, or pulling actions to disperse and distribute the solid component [1]. In the case of Polymer Bonded eXplosive (PBX) manufacture, it is necessary to distribute crystalline high explosive filler particles (along with other ingredients such as plasticiser, additives, and curative) throughout a liquid rubber prepolymer, and cast the resultant mixture into a warhead or bomb case. Homogeneity is important to ensure the properties of the material are consistent throughout its volume, which optimises its properties [2].

During PBX manufacture, the high shear mixers typically employed are planetary or z-blade mixers, which consist of orbiting blades that move in close contact to maximise shear, or horizontally rotating 'z' or 'ς' (sigma) shaped blades that knead the material respectively [1–5]. However, conventional high shear mixing of this type has drawbacks such as mix times of up to several hours, and the production of waste on the order ~12.5% of the mix mass since the mixing vessel and blades must be cleaned after use [6].

Resonant Acoustic Mixing (RAM) has recently garnered substantial interest as an alternative to conventional high shear mixers for use in the manufacture of cured PBXs [7]. Instead of mixing blades, the apparatus consists of a vertically vibrating spring-mounted platform to which a mixing vessel is affixed. The oscillations occur at a peak acceleration up to 100 G, where G is acceleration due to Earth's gravity (9.81 m s^{-2}), with an amplitude up to 1.4 cm peak-to-peak. The frequency is held at the mechanical resonance of the system, approximately 60 Hz, with energy conveyed to the mixture through longitudinal acoustic pressure waves (vibrations). This is claimed to result in uniform medium shear mixing over the entire volume of the mixing vessel, as opposed to high shear mixing localised to the vicinity of mixing blades [8,9]. Advantages of RAM over conventional techniques are said to include mixing times orders of magnitude shorter [9], reduced cleaning requirement and associated waste, and the concept of mixing 'in-situ' [10], whereby the intended casing of the cured product doubles as the mixing vessel. This potentially allows for the manufacture of high

* Corresponding author.
E-mail address: g.kister@cranfield.ac.uk (G. Kister).
[1] Present address: BAE Systems Land (UK), Glascoed, Usk, NP15 1XL, United Kingdom
[2] Present address: High Energy Materials Research Laboratory, Sutarwadi, Pune, 411021, India
[3] Present address: Roxel (UK Rocket Motors) Ltd., Summerfield, Kidderminster, DY11 7RZ, United Kingdom

https://doi.org/10.1016/j.cep.2022.108806
Received 1 October 2021; Received in revised form 31 December 2021; Accepted 21 January 2022
Available online 7 February 2022

viscosity novel PBX formulations that would otherwise be difficult to cast, and removes the requirement for cleaning. However, the mixing mechanism is still poorly characterised in comparison to conventional methods. In order for the full potential of RAM to be realised, a better understanding of the factors that determine mixing efficiency (time and energy required for homogeneity) must first be sought.

1.1. Mixer operating principle

One of two parameters can be defined by the user to control a mixing cycle — set peak acceleration of the vibrating plate up to 100 G, or set mixer 'intensity' up to 100%. 'Intensity' here refers to applied current to the driver motor up to 5 A,[4] and by extension, peak driving force. Mixer 'intensity' is commonly referred to as 'power' or 'power intensity' by the manufacturer. The operation of the system can be simplified to that of an under-damped driven harmonic oscillator [8], where the relation between acceleration and driving force is given as:

$$m\frac{d^2}{dt^2}x(t) + c\frac{d}{dt}x(t) + kx(t) = Fsin(2\pi f_d t) \quad (1)$$

where m is the mass of the system (kg), $x(t)$ is the displacement of the plate as a function of time (m), c is the damping coefficient (kg s^{-1}), k is the spring constant (N m^{-1}), F is the peak driving force (N), f_d is the driving force (resonant) frequency (Hz), and t is time (s). The inertial force (product of mass and acceleration), damping forces (losses from mixing and non-ideal losses), and stored forces constitute the first three terms, while the driving force constitutes the final term. Inertial and stored forces cancel out over each oscillation period since the system is held in resonance by the control software.

As mixing progresses and the rheology of the material changes, so too does the energy required for mixing, and the associated damping coefficient, c. Therefore the variables which balance the equation must also vary over a mixing cycle. This means that for a set acceleration or set mixer 'intensity', there will be a corresponding achieved mixer 'intensity' or acceleration, depending on the 'mixing forces' (and non-ideal losses) present at any particular instance.

1.2. Movement modes

Initially, when the components to be mixed are separated into layers, the introduction of solid components into the liquid components (termed the 'wetting stage' by Lucon et al. [11]) has been attributed to Faraday instabilities. These non-linear waves on the surfaces of liquids occur under high amplitude periodic driving forces, and are reported by the manufacturer to manifest as 'fingers' or 'spikes' above the liquid surface, or 'cavities' below it. Videos of the phenomenon are available on the manufacturer's website [8,9]. It is said that the presence of these instabilities at the boundary between materials of different density (i.e. layers of material) is responsible for the rapid wetting observed. The mixing effect of instabilities was investigated computationally for two viscous liquid layers (HTPB resins) by Nance [12,13], whereby the associated vortices and eddy currents were modelled. The presence of particles was however omitted, and it was cautioned that the underlying physics requires further investigation to be better understood.

Provided the material has sufficient inertia to move (non-quiescent conditions [14]), several movement modes are possible as mixing progresses through 'incorporation', whereby the solids and liquids become better integrated, and 'mixing', whereby the mixture becomes fully homogenised [11], depending on the rheology of the material and applied conditions [11,14–16]. An undesirable movement mode is 'decoupled', whereby lumps of material levitate or bounce around the interior of the vessel [14]. Conversely, a preferable movement mode is 'churning' [14,16], whereby the vessel contents couple to the vessel wall, ideally with a 'no-slip' condition at the interface. Over an oscillation period starting from displacement minima, the bulk of the material is given inertia in the upwards direction. Upon the changing direction of the oscillation (at the apex of the plate displacement), the mixing vessel immediately changes direction, while the bulk of the material does not immediately respond. As a result, a velocity gradient facilitated by the viscosity of the material, which allows adjacent layers of material to 'adhere' to each other, extends perpendicularly across the material towards the centre [11,14,17], resulting in a bulk rolling motion which provides the shear required for effective mixing [16]. Vigorous churning is referred to as 'bulk mixing' by the manufacturer [11,14], and has widely been suggested as the most desirable movement mode for highly loaded suspensions. It therefore follows that mixing efficiency will rely on the amount of movement in the material and the degree to which the 'no-slip' condition is fulfilled. By maximising movement and minimising wall slip, the velocity gradient, thus shear, will increase.

Table 1
The salient factors affecting the efficiency of churning [18].

Reduces wall-slip	Increases movement
	Higher acceleration [16,19,20] Higher density [20,21] -Greater inertial forces
Higher viscosity [20–22] -Greater drag -Greater tackiness	Lower viscosity [20–22] -Greater compliance
Smaller diameter [11,20,23] Optimised roughness [18] -Greater drag	Larger diameter [11,20,23] -Greater compliance
Lower surface tension [18] Higher surface energy [24] -Greater spreadability	Lower surface tension [18] -Greater compliance
	Vacuum application [16,21,22] -Greater inertial forces -Greater compliance

1.3. Maximising efficiency

The amount of both slip and movement has been reported to rely on the factors given in Table 1. Properties such as viscous drag, tackiness (or 'stickiness'), and binder spreadability enhance wall coupling, while greater inertial forces and greater compliance within the material enhance the degree of movement. Since PBXs should ideally be designed to optimise final properties rather than mixing properties, variables relating to the formulation (viscosity, density, surface tension etc.) should be treated as incidental factors. The main focus should instead be given to maximising efficiency using variables related to the machine (acceleration) and vessel (surface free energy, roughness, diameter, and vacuum application). The aim of this work is to further examine three of these variables: acceleration, vacuum application, and vessel surface free energy. Consistency between three mixer units is also investigated.

1.4. Effect of acceleration

The degree of movement in the vessel contents will depend on the ratio of inertial forces, where greater inertial forces deform the material more, to viscous forces, where lower viscosity makes the material more compliant, and can be described by the vibrational Reynolds number. Using an inert PBX simulant mixture with known viscosity and mixing vessels of six different diameters between 9.7 mm and 82.6 mm, Coguill

[4] In the case of the LabRAM (original model), as used in this work.

and Martineau [20] found that the onset of churning as acceleration was increased could be described by an empirical relationship:

$$\frac{Re_v}{D} > 87(10^3 D)^{-0.9} \quad (2)$$

where Re_v is vibrational Reynolds number (dimensionless), and D is vessel diameter (m). The relation as given in the original text has here been augmented with a conversion factor (10^3), so that D can be considered in consistent units. It should however be noted that the relation is not dimensionally consistent without the empirically derived coefficient (87) also having units of its own. By inspection, the units should take the non-standard form of $m^{-0.1}$. Furthermore, the methodology and parameters with which the viscosity of the mixture was determined were not stated in the text. Highly loaded suspensions are invariably non-Newtonian thus have a shear rate dependent viscosity. The viscosity as was measured may therefore have not corresponded with that of the material when mixing under the different parameters, meaning the calculated Reynolds numbers used to derive the empirical coefficients may not have been strictly accurate. Determination of the shear rates during mixing to apply adjusted values for viscosity would have however posed a challenge in itself.

By substituting an expression for vibrational Reynolds number, an expression for efficient mixing is apparent in the form of:

$$\frac{a\rho(10^3 D)^{0.9}}{87(2\pi)f\eta} > 1 \quad (3)$$

where a is the applied acceleration (m s^{-2}), ρ is density (kg m^{-3}), D is vessel diameter (m), f is vibrational frequency (Hz), and η is absolute viscosity (Pa s), which is again for an unknown shear rate and discounts non-Newtonian effects. It should also be noted that the equations do not account for the effects of vacuum application, surface tension, or wall-slip. These factors are further discussed later in this review.

Regardless, it is still clearly apparent that for a given experimental set-up, higher acceleration, thus greater inertial force, is beneficial for the effectiveness of churning. Work by Lucon et al. [11,14] has indeed shown that higher acceleration increases the rate of energy supplied to the mixture, with the caveat that unintended changes in mixing mode (from churning to decoupled in shear thickening fluids) must be avoided. Since imparted energy has been correlated to the degree of homogeneity when considering both RAM [25] and conventional mixing [26], it would follow that higher acceleration leads to reduced mixing time. However, this has not been quantitatively reported. From the relation, it is also apparent that larger vessel diameter, greater formulation density, and lower viscosity are beneficial for churning, as summarised in Table 1.

1.5. Effect of mixer unit

There are several mixer models available depending on scale, as summarised in Table 2. All but the two largest models (which are driven by eccentric masses) are driven electromagnetically by a voice coil, though the principle of mixing is the same regardless of the size or configuration of mixer used. It may however be expected [20] that larger capacity vessels will present differences in mixing behaviour due to a decreasing vessel surface area to mixture volume ratio. That is to say that for wider vessels, the viscous forces at the wall become small compared to the inertial forces on the mixture, in essence making the material more compliant [11]. Use of larger capacity vessels when scaling up has also been reported to hinder thermal dissipation [27], likely again due to a lower surface area to volume ratio.

It is unclear what differences may be apparent between different units of the same mixer model, though manufacturing variation in the components used (driver motors, accelerometers, springs etc.) and design iterations may result in discrepancies. Calibration may also differ between machines.

Table 2
Comparison of maximum fill capacity and maximum power to mix for each mixer model using the manufacturer's standard mixing equipment [28,29].†Denotes a discontinued model.

Bench scale	LabRAM†	LabRAM I	LabRAM II
Capacity (g)	500	500	1000
Power (W)	37	410	640
Production scale	**OmniRAM**	**RAM 5**	**RAM 55**
Capacity (kg)	5	36	420
Power (kW)	4.1	23.2	244

1.6. Effect of vessel material

It has been reported anecdotally that mixing in PTFE (Teflon™) vessels results in reduced efficiency and poor mix quality [24]. This was attributed to PTFE's low surface free energy of <20 mJ m^{-2} [30] causing poor adhesion to the mixture, thus ineffective wall coupling (significant slip). Mixes performed in vessels made out of higher surface free energy polymers[5] (30–50 mJ m^{-2} [30]) and metals[6] (~40 mJ m^{-2} for simple cleaning treatments [31], though nominally hundreds of mJ m^{-2} [32]) have not been reported to cause such problems.

In order for wall slip to be minimised, it would be expected that material at the interface must prefer to stick to the wall (adhesion) rather than move with the bulk of the material (cohesion). In the context considered here, the surface tension of the binder components will act as a cohesive force, and the work of adhesion between the binder components and vessel surface (the energy required to separate the two phases) will act as an adhesive force. The surface free energy of the vessel wall and surface tension of the binder mixture will both directly influence work of adhesion, as shown in the Owens–Wendt–Rabel–Kaelble (OWRK) [33–35] equation:

$$W_A = 2\left(\sqrt{\sigma^d_{SFT}\sigma^d_{SFE}} + \sqrt{\sigma^p_{SFT}\sigma^p_{SFE}}\right) \quad (4)$$

where W_A is the work of adhesion, σ_{SFT} denotes the surface tension of the binder mixture, σ_{SFE} denotes the surface free energy of the vessel material, and d and p denote the dispersive and polar components thereof. All have units of mJ m^{-2}.

It is therefore postulated that a surface and binder combination which provides a higher work of adhesion to surface tension ratio will reduce wall slip, thus increase the velocity gradient and improve mixing efficiency. Higher ratios of this nature are reflected in lower droplet contact angle between the liquid and solid, as shown in the Young–Dupré [36] equation:

$$\theta = cos^{-1}\left(\frac{W_A}{\sigma_{SFT}} - 1\right) \quad (5)$$

where θ is the expected contact angle (degrees), W_A is the work of adhesion (mJ m^{-2}), and σ_{SFT} is the surface tension of the binder mixture (mJ m^{-2}). It is apparent that by increasing the surface free energy such that the work of adhesion increases, without modifying surface tension, the contact angle will decrease.

While the above paragraphs address the effect of 'true' slip at the molecular level, also of consequence may be 'apparent' slip. Here, a lubricating binder rich layer is formed at the vessel wall since the filler is unable to penetrate it, locally diminishing the volume fraction. Apparent slip can be mitigated with textured surfaces which are able to interact directly with the bulk material [37], though attempts to recreate this with RAM have initially proved unsuccessful [18]. Practically speaking, the use of textured mixing vessels may be unsuitable for batch RAM where there is requirement for cleaning, though the technique may be viable when mixing 'in-situ'.

[5] Such as polycarbonate (PC), polystyrene (PS), and poly(methyl methacrylate) (PMMA).

[6] Such as stainless steel, titanium, and aluminium.

1.7. Effect of vacuum

Another variable which can be considered over a mixing cycle is vacuum application. Yew et al. [22] found that partial vacuum substantially reduced the time required for homogeneity to be achieved, attributing the observation to lower air pressure in the sealed mixing vessel reducing resistance against bulk flow. A similar explanation has been given by Lucon [17], though in this case, the induction of bubbles in the material due to partial vacuum application was also reported to have the effect of making the material more compliant. With greater compliance, it would be expected there would be greater movement within the material, thus a larger velocity gradient and greater shear. When subjected to acoustic pressure waves, it is also said [11] that the oscillation of entrapped air bubbles influences the flow of the surrounding liquid (acoustic microstreaming), enhancing the mixing process. This phenomenon is referred to as 'bubble pumping' in the RAM patent [38,39]. It has however been forewarned by Yew et al. [22] and others [17] that premature application of vacuum can cause unmixed material to be evacuated from the mixing vessel. The incremental reduction of pressure has subsequently been found to mitigate this. In all, the aforementioned studies suggest the presence of gas bubbles brought about by partial vacuum application is beneficial for mixing.

With this in mind, it would follow that premature degassing of the mixture is not beneficial. McCloy et al. [16] found that vacuum application over extended periods of time had the effect of impeding the mixing process after initially aiding the process, attributed to the gradual loss of air bubbles by evacuation. Similarly, Lucon [17] states that the removal of air bubbles with hard vacuum will lessen the compliance of the material (i.e. make it more difficult to move), resulting in the reduction of the velocity gradient required for shear generation. It therefore follows that hard vacuum for degassing purposes should be reserved for the final stages of a mixing sequence, where evacuation of air is specifically required to prevent the inclusion of voids within the cured material.

1.8. Monitoring mixing progression

When mixing at constant acceleration, the 'wetting', 'incorporation', and 'mixing' stages described by Lucon et al. [11] were linked to varying mixer 'intensity'. Large and rapid variations were apparent in the wetting stage, likely due to the homogeneity, thus damping coefficient (see Eq. (1)), quickly changing. During the incorporation stage, where the solid and liquid phases became cohesive and resisted flow, low 'intensity' was recorded. Upon the mixture becoming more fluidised and churning becoming apparent, 'intensity' increased again as efficient mixing meant more energy was imparted into the mixture.

Mixing evolution was also examined by Vandenberg and Wille [19], where concrete mixing was under investigation. When considering a mixing cycle at constant 'intensity', it was found that five characteristic stages of mixing (defined by the force dissipation mechanisms believed to be occurring in the mixture) corresponded with five discrete sections of the acceleration response profile. The concrete mixing acceleration profile (average of three) is reproduced in Fig. 1. The mixing stages and corresponding dissipation origin forces are; a- 'dry granular' mixture (friction), b- 'wet granular' mixture (friction/cohesion), c- 'hard paste' (cohesion), d- 'soft granular fluid suspension' (cohesion/viscous), and upon homogeneity being achieved, e- 'fluid suspension' (viscous).

It would appear that stage 'a' corresponds to a wetting stage, stages 'b' and 'c' correspond to an incorporation stage, and stages 'd' and 'e' correspond to a mixing (churning) stage. These findings suggest that mixing progression with RAM can be effectively monitored by interpretation of acceleration or 'intensity' readouts.[7] Specifically for the churning movement mode (where the shear rate, thus vigorousness of mixing is determined by the factors listed in Table 1), it would be expected that the mixer 'intensity' (i.e. power requirement from the mixer) will depend on the magnitude of the shear rate, with an additional dependency on the compliance of the material (where greater compliance will require less power to maintain an equivalent shear rate).

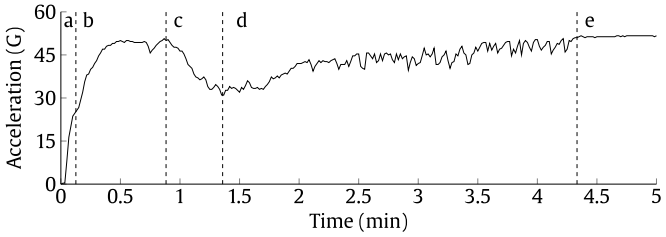

Fig. 1. The average acceleration profile for concrete mixing (concrete mix 91% w/w, water 9% w/w) at 50% mixer 'intensity' reproduced from Vandenberg and Wille [19]. Vacuum was not applied.

1.9. Energy determination

When the mixing vessel is not filled, the system acts as a rigid body mass. In this case, any damping is purely consequential of non-ideal losses in the system, such as air resistance, friction, and noise. Once filled, additional losses are attributed to work done in mixing the material. When using conventional high shear techniques, the energy consumed for mixing can be deduced by integrating the power supplied to the mixture, where power can be derived at any given time from measurements of impeller shaft torque [2,26]. It would be expected that analogous methods could be employed with RAM.

Using Newtonian mechanics, the manufacturer has developed an equation to determine power consumption. The method is valid for the LabRAM (original) mixer model [40,41], and has been previously applied in academic studies [19,42]. Over the duration of a mixing cycle, the energy supplied to the mixture can be given by:

$$E_{EOM} = \sum_{t_0}^{t_{EOM}} P_{mix}(t)\Delta t \tag{6}$$

where

$$P_{mix} = \left(\mathcal{F}\frac{\Delta I}{100}\right)\left(0.707\frac{a}{2\pi f}\right) \tag{7}$$

where E_{EOM} is the total energy consumption to the end of mix point (J), $P_{mix}(t)$ is the power to the mixture for any given time (W), Δt is the time increment where P_{mix} is valid (s), t_0 and t_{EOM} are the start and end times respectively (s), $\mathcal{F}$ is an empirically derived LabRAM constant (70 ± 4 N), ΔI is the difference in mixer 'intensity' between when unfilled (baseline) and filled (%), a is peak acceleration (m s^{-2}) with a statistical correction factor to root mean square acceleration (0.707), and f is vibrational frequency (Hz).

The following sections report and discuss the influence that acceleration, vacuum, and mixing vessel material have on the efficiency of mixing. A method to monitor the stages of mixing based on the mixer 'intensity' is presented, together with a discussion of reproducibility of mixing between mixer units. Finally, a combined theory of movement modes is presented and discussed.

2. Materials and methods

2.1. Formulation

An idealised inert simulant formulation based on glass microbeads filler (Glass Sphere s.r.o., Czech Republic, see Table 4), hydroxy-terminated polybutadiene (HTPB) binder (type Poly bd® R-45 HTLO,

[7] Similar methods are indeed used with conventional mixing, where since torque is related to viscosity [26], the point of constant torque can be considered the point of constant viscosity.

Table 3
The glass microbead formulation used for mixing.

Loading	Glass	DEHA	HTPB
Volume (%)	62.00	19.00	19.00
Actual mass (%)	81.65	9.30	9.05
RDX equivalent mass (%)	76.49	11.91	11.60

Table 4
Density (Micromeritics AccuPyc 1330, five measurements) and particle size analysis (Cilas 1190, dry mode, three measurements) of the glass microbeads. ±1 standard deviation stated.

Density (g cm^{-3})	D10 (μm)	D50 (μm)	D90 (μm)
2.4905 ± 0.0002	12.7 ± 2.3	28.3 ± 1.7	45.4 ± 1.5

Table 5
The large glass bead formulation used for vacuum observations.

Loading	Glass	HTPB
Volume (%)	62.00	38.00
Actual mass (%)	81.85	18.15
RDX equivalent mass (%)	76.72	23.28

Table 6
Density (Micromeritics AccuPyc 1330, five measurements) and particle size analysis (optical analysis 50 × magnification) of the large glass beads. ±1 standard deviation stated.

Density (g cm^{-3})	Diameter (mm)
2.4890 ± 0.0173	1.20 ± 0.08

Cray Valley, USA), and di(2-ethylhexyl) adipate (DEHA) plasticiser (≥ 97%, Merck, UK) was used to perform the mixing experiments, and is given in Table 3. Drop shape analysis was used to characterise the DEHA/HTPB binder mixture using standard methods described in Appendix A. Curative was not used since only the mixing behaviour was of interest, and not the properties of the final composite. The viscosity of the mixture was analysed at the end of a mixing cycle using a TA Instruments HR-1 rheometer, with 25 mm parallel plates at a 500 μm gap height, a 2.5 s^{-1} shear rate, and a 2 °C per minute heating rate.

2.2. Mixing vessels

Mixing vessels (48 mm diameter and 47.5 mm height, with rounded internal edges to minimise mixing dead spots) were milled from PTFE, PMMA, and Grade 5 titanium[8] blocks. A 15 mm thick insulating plastic (polyoxymethylene) base plate was also used in the case of titanium, in an attempt to normalise its thermal behaviour to that of the less conductive plastic vessels. The differing masses of the vessels were normalised by attaching dead weights (washers) to the vibrating plate when the lighter vessels were being used. The baseline mixer 'intensity', associated with non-ideal losses, would otherwise vary between vessels unintentionally.

Surface samples of each vessel material were also characterised using drop shape analysis, again using standard procedures described in Appendix A. Each sample was first exposed to binder mixture before being thoroughly washed twice using dish soap and water, and dried with paper towels, in the same cleaning procedure as the mixing vessels.

2.3. Mixing procedure

For all mixes undertaken, the ingredients were weighed directly into the vessel at the start of each mixing cycle (so-called 'one-shot' mixing), with the first half of the filler being followed by the plasticiser, and the second half being followed by the binder. A total fill of 65 ml of the formulation was used. LabRAM 'A' was used for mixing unless stated otherwise, and was controlled via aftermarket devices and software supplied by The Falcon Project Ltd., which allowed for machine control at constant acceleration setting, temperature logging, and vacuum control. A rod thermocouple was inserted into the centre of the mixture through an airtight portal in the vessel lid. The vessel lid was of custom design and PEEK[9] construction, and was held in place with a clamshell clamp. The pressure in each vessel was slowly reduced to 550 mbar (partial vacuum) in 12 s duration increments of 25 mbar before the start of mixing, to prevent evacuation of material into the vacuum lines.

[8] 90% titanium, 6% aluminium, 4% vanadium.
[9] Polyether ether ketone.

2.4. Mixing experiments

The baseline mixer 'intensity' required to vibrate a rigid body mass equivalent to a filled vessel (604 g) was determined on each LabRAM mixer unit ('A', 'B', and 'C') for the acceleration setting(s) under investigation. For the PMMA vessel (transparent), three mixes of the formulation were performed using LabRAM 'A' at 45 G, 50 G, and 55 G. An additional three mixes were performed at 50 G using LabRAM 'C'. Three mixes (two in the case of titanium) were then undertaken at 50 G in the PTFE and titanium vessels using LabRAM 'A'.

The cooling behaviour of the mixture was recorded for each of the PMMA, PTFE, and titanium vessels once the machine was turned off, and analysed between 45 °C and 35 °C using the linear form of Newton's Law of Cooling. The expression for kt was plotted against time.

$$kt = -ln[(T(t) - T_{amb})/(T_0 - T_{amb})] \quad (8)$$

where k is the cooling constant (min^{-1}), t is time (min), $T(t)$ is vessel internal temperature as a function of time (°C), T_{amb} is the ambient temperature (°C), and T_0 is the initial vessel internal temperature (45 °C). The cooling constant, k, which was used as an empirical parameter to compare the thermal behaviour between the vessels, was found by taking the gradient of the line.

A slightly different approach was used to determine the effect of vacuum, whereby large glass beads (Glass Sphere s.r.o., Czech Republic, see Table 6) were loaded (62% v/v) into both fresh HTPB binder and completely degassed HTPB binder respectively (80 ml of formulation in each case) as shown in Table 5. An acceleration of 90 G was then applied, and pressure reduced incrementally to 100 mbar. Mixer 'intensity' and movement observations were recorded.

3. Results and discussion

3.1. Mixing progression

A mixer 'intensity' profile and corresponding temperature increase (above ambient) profile is shown in Fig. 2. The horizontal dotted line shows the measured mixer 'intensity' readout (36.8%) for an equivalent rigid body mass vibrated at the same acceleration (50 G), and accounts for the mixer 'intensity' required to overcome non-ideal losses (baseline mixer 'intensity').

Immediately after the mixer was switched on, the vessel contents were still fully segregated into layers from the loading procedure. Wetting (W), whereby the solids were introduced to the liquids, then occurred rapidly up to 0.7 ± 0.1 min, where the large fluctuations in mixer 'intensity' were indicative of the rapidly changing rheological state [11]. Wetting was followed by an incorporation (I) stage up to 9 ± 1 min. Decoupled movement was initially observed here, where the material formed cohesive lumps that bounced around the vessel interior. As the solids and liquids became more uniformly distributed and fluidised with time, the movement mode seemed to rapidly switch

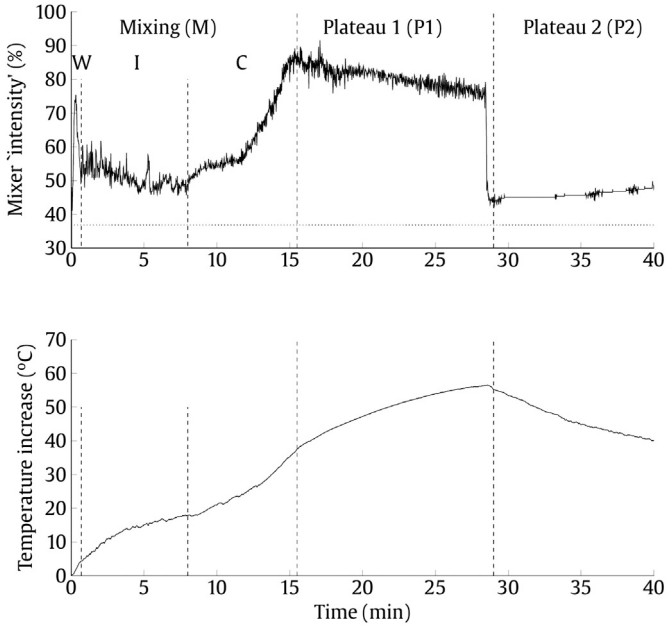

Fig. 2. Example mixer 'intensity' and temperature increase profiles up to 40 min of mixing for the glass microbead formulation. Glass microbeads 62% v/v, DEHA 19% v/v, HTPB 19% v/v, 65 ml, 550 mbar pressure, 50 G acceleration, PMMA vessel, LabRAM 'A'. The average ambient temperature over this mix and two repeats was 21 ± 1 °C.

between decoupled and attempts at churning, whereby the material would briefly couple to the wall before detaching again.

Churning (C) was the only movement mode subsequently observed, with the emergence of a favourable wall coupling condition upon the material becoming further fluidised likely responsible. This stage would correspond to the 'mixing' stage as described by Lucon et al. [11]. The churning became faster and more vigorous in this stage, probably due to the temperature increase lowering the viscosity (thus increasing the compliance) such that a larger velocity gradient across the material was made possible. With a larger velocity gradient, increased shear, thus energy expenditure, was likely responsible for mixer 'intensity' readout, thus power consumption, building to its overall maximum at 17 ± 2 min. This was accompanied by a further temperature rise that steepened as mixer 'intensity' increased. The profile up to this point (stages W, I, and C) is herein referred to as the mixing stage (M), whereafter homogeneity was no longer observed to be changing.

Between 17 ± 2 and 29 ± 1 min there was a high mixer 'intensity' churning stage where the profile formed a plateau (P1). In temperature controlled vessels, it has been reported that such plateaus upon mixing completion remain horizontal [43]. However, in this case, without external temperature control, it would appear the steadily increasing temperature had a net effect of lowering the mixer 'intensity', possibly due to an increasing amount of wall slip and/or a lower power requirement to maintain the shear rate as viscosity further reduced. Temperature reached its maximum point at the end of this stage, whereafter there was a sharp drop in mixer 'intensity'. The profile then formed a second plateau (P2), a phenomenon that has not previously been reported. A possible explanation may be a readjustment in the churning movement mode of the material. Once the temperature reached an absolute value of 75.6 ± 0.4 °C, the viscosity of the material used may have lowered to a 'tipping point' whereby the material no longer possessed adequate viscous drag to couple to the vessel wall and/or sustain the velocity gradient across the material, leading to a collapse in the movement mode. Vessels that are temperature controlled to slightly below this point may therefore prevent the P1–P2 transition. Conversely, vessels temperature controlled above this point, or to the temperature at the start of the churning stage - C, may

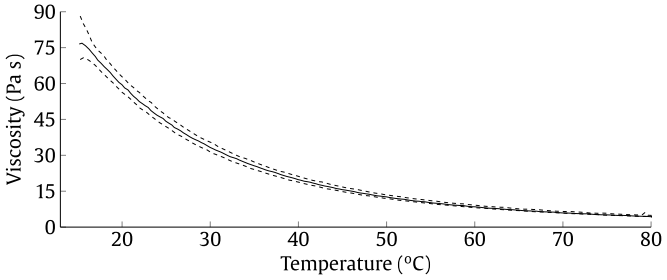

Fig. 3. Glass microbead formulation viscosity analysis taken at the end of a mixing cycle. ±1 standard deviation shown. Glass microbeads 62% v/v, DEHA 19% v/v, HTPB 19% v/v.

preclude the 'intensity' build up to the P1 stage altogether. The effects of these conditions should be investigated as future work.

The fact that the P1–P2 transition was not apparent in Fig. 1 for concrete (where the vessel was also not temperature controlled) could be because of its already low viscosity (~4 Pa s), and/or a more temperature dependent rheology when mixing polymers. The viscosity of a generic cement slurry has been shown [44] to fall by <5% between 20 °C and 40 °C (a typical end of mix temperature observed by Vandenberg and Wille [19]), whereas Fig. 3 shows that the polymer-bound formulation used here falls by 67% across the same range. Changes in viscosity due to both homogeneity and temperature are therefore of importance when PBX mixing, meaning the viscosity, thus mixer 'intensity' reading, may still be changing beyond the time at which homogeneity is achieved. In any case, it would appear direct comparisons in mixing behaviour between polymer suspensions and concrete mixtures are difficult to make due to their significantly different rheologies.

During the P2 stage, it was seen visually that churning was still occurring, albeit at lower mixer 'intensity' than in the P1 stage. Despite the decreasing temperature in this stage, energy was still being supplied to the mixture as was reflected in the positive difference between the profile and the dotted line at the mixer 'intensity' measured for an equivalent rigid body mass. This would suggest the lower mixer 'intensity' corresponded to less vigorous churning, such that the rate of cooling exceeded the rate of heating. It would appear the system tended towards a steady equilibrium, where the effects of temperature (thus viscosity), velocity gradient, and power draw became balanced. The absence of a subsequent build-up of mixer 'intensity' to that seen before the P2 stage as the material cools (thus viscosity increases again) could be explained with the fact that more than one coupling condition/movement mode can be apparent under the same conditions [14]. Those coupling conditions/movement modes in this case would be high and low mixer 'intensity' churning, and those same conditions would be 'mixedness' and temperature.

While quantitative analysis of changing homogeneity was not undertaken throughout the mixing cycle, visual observation would suggest mixing completion occurred somewhere between churning becoming the only mixing mode observed (C) and the mixer 'intensity' peak (M–P1 transition). The latter makes an excellent reference feature to take as the end of mix point, and is herein referred to as such. The duration of the P1 stage also provides an insight into the rate of energy uptake once vigorous churning is fully established. For investigating the underlying factors affecting RAM efficiency using idealised systems (or when live explosives mixing is impractical), the formulation is therefore recommended for future use.

3.2. Effects not considered

Non-idealised formulations used for PBXs may be expected to present different mixing profiles than observed here. High explosive

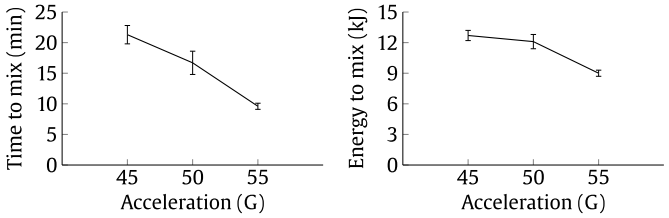

Fig. 4. Line graphs showing the average time (left) and energy (right) required for the end of mix point at 45 G, 50 G, and 55 G acceleration over triplicate measurements. Glass microbeads 62% v/v, DEHA 19% v/v, HTPB 19% v/v, 65 ml, 550 mbar pressure, PMMA vessel, LabRAM 'A'. ±1 standard deviation shown. The average ambient temperature for the nine mixes was 22 ± 1 °C. Full mixing data is given in Appendix B.

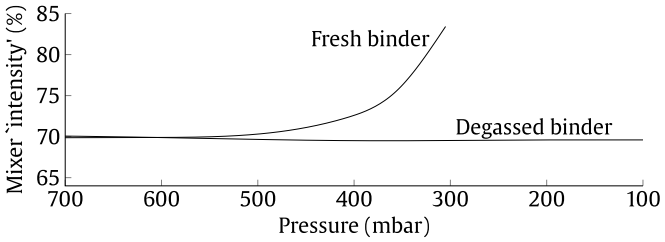

Fig. 5. Comparison of mixer 'intensity' against pressure reduction for degassed and fresh binder. Large glass beads 62% v/v, HTPB 38% v/v, 80 ml, 90 G acceleration, PMMA vessel, LabRAM 'A'.

fillers typically used in PBXs have wide particle size distributions (such as the 'Class 1' RDX[10] industry granulation standard which ranges from <75 to 850+ μm [45]), are irregular in shape, and are included at considerably higher loadings (typically ~88% w/w). As such, real formulations have a higher viscosity that may preclude the P1–P2 transition or the high 'intensity' observed in the P1 stage. In this eventuality, higher acceleration, stronger vacuum, or external heating may need to be applied. Runaway temperature increases from greater frictional heating should however be avoided.

Curative was also not included in the formulation for this study. While curative would be initially expected to plasticise the formulation, after a time of typically several hours known as pot-life, the viscosity would rise again due to the cross-linking reaction taking place. Though an important consideration for conventional mixing, pot-life is unlikely to affect RAM due to the much shorter timescales required. The formulation also did not contain processing aids, bonding agents, or other minor ingredients commonly added to PBXs, which may also influence the viscosity and wetting characteristics of the formulation/binder. A more thorough review of the effects of formulation variables on mixing has been presented previously by the authors [18].

3.3. Effect of acceleration

Fig. 4 shows the average time and energy (Eq. (6)) required for the end of mix point over the three mixes performed at each acceleration. It is apparent that higher acceleration corresponds to more rapid mixing. The average time required reduced by 55% upon an increase in acceleration from 45 G to 55 G, and 43% between 50 G and 55 G.

While it would be expected that mixing time will be shorter at higher accelerations (since more energy is imparted on the vessel contents at any given time), the total amount of energy required to mix the material may be expected to remain constant, i.e. a certain amount of energy would be required to rearrange the vessel contents. However, Fig. 4 shows that the total energy required for the end of mix point is lower when at higher acceleration. This may be due to the more vigorous mixing at higher acceleration more rapidly increasing the temperature, reducing the viscosity of the formulation which then requires less energy to mix. This effect may be further exacerbated by shorter mix times at higher acceleration allowing less time for the vessel to lose heat to the surroundings, further increasing the rate of viscosity reduction.

3.4. Mixer to mixer reproducibility

LabRAM 'B' and 'C' were found to maintain a higher baseline mixer 'intensity' of 40.5% and 51.6% respectively (as opposed to 36.8% for LabRAM 'A') when run with the rigid body mass at a set acceleration of 50 G. Mixing was undertaken with LabRAM 'C', the machine with the largest discrepancy. Though consistent with LabRAM 'A' in shape, the mixing profiles exhibited a consistently higher mixer 'intensity' throughout. Mixing (and temperature increase) was found to be considerably faster, with the end of mix point occurring after 9 ± 2 min as opposed to 17 ± 2 min for LabRAM 'A'. This was despite the acceleration set point and ambient conditions being consistent between the mixers. Full mixing data is given in Appendix B.

It is believed that accelerometer calibration was the main cause of the discrepancy between units, although there may also have been further variation in motor efficiency, plate mass, and spring constant. Although the LabRAM (original model) used in this work has now been discontinued, it is recommended proper characterisation and calibration of all machines (perhaps using additional accelerometers) should be performed by researchers and industry. This will ensure mixing behaviour and product outcome are consistent across all units, models, and control methods intended to perform reproducible mixing cycles.

3.5. Effect of vacuum

A plot of mixer 'intensity' against reducing pressure at a fixed acceleration of 90 G is shown in Fig. 5. Note that 80 ml of different formulations containing much larger beads (1.20 mm diameter) in pure HTPB were used in this experiment.

The formulation containing fresh HTPB started to show obvious signs of mixing at a pressure of 400 mbar, while the formulation consisting of completely degassed HTPB did not exhibit any mixing at any applied pressure. This corresponded to the mixer 'intensities' recorded in Fig. 5, where a marked increase in 'intensity' was apparent upon mixing onset, increasing further as pressure continued to reduce. These findings are in good agreement with McCloy [16] and Lucon [17], which suggested that partial vacuum, thus bubble induction increasing compliance, assists churning, while degassing the binder, thus removing the compliance, does not. While surely beneficial, vacuum application should not however be considered imperative for mixing real systems, with mixing completion being reported in the absence of vacuum [19].

3.6. Effect of vessel material

The time to the end of mix point and the energy supplied up to that point for mixing in PTFE, PMMA, and titanium are shown in Fig. 6. Mixing in PMMA and titanium as opposed to PTFE resulted in a 17% and 16% reduction in time to mix, and 6% and 4% reduction in energy to mix respectively. However, due to overlapping error bars combined with small sample sizes, the significance of the reductions cannot be determined. It is recommended that the experiment be repeated with a larger sample size and a variety of formulations as future work to provide a definitive conclusion. The data presented does however give a preliminary indication that low surface free energy vessels reduce the effectiveness of RAM, in line with previous observations [24].

[10] 1,3,5-trinitro-1,3,5-triazinane.

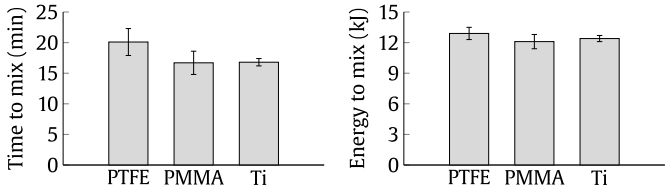

Fig. 6. Bar graphs showing the average time (left) and average energy (right) required for mixing completion in PTFE, PMMA, and titanium vessels over triplicate, triplicate, and duplicate measurements respectively. Glass microbeads 62% v/v, DEHA 19% v/v, HTPB 19% v/v, 65 ml, 550 mbar pressure, 50 G acceleration, LabRAM 'A'. ±1 standard deviation shown. The average ambient temperature for the eight mixes was 22 ± 3 °C. Full mixing data is given in Appendix B.

Table 7
The disperse and polar components of the surface free energies and surface tensions, and the expected contact angles between them. The surface free energy values for PTFE and PMMA are generally in good agreement with literature values of 19 mJ m^{-2} [33] and 40 mJ m^{-2} [46] respectively.

Material	σ^d (mJ m^{-2})	σ^p (mJ m^{-2})	σ (mJ m^{-2})	θ_c (degrees)
Binder	20.6	9.1	29.7	–
PTFE	18.9	0.1	19.0	70
PMMA	30.0	3.3	33.3	0
Titanium	28.4	8.7	37.1	0

Table 7 shows the surface tension of the binder mixture and the surface free energies of the vessel materials, along with their expected contact angles with the binder mixture (from Eq. (5)). As anticipated, the PTFE surface had a significantly lower surface free energy than the PMMA and titanium surfaces, resulting in an expected contact angle of 70° as opposed to total spreading in the other cases. This would account for the observation that the PMMA and titanium vessels gave similar mixing times, while mixing in the PTFE vessel took longer. Low surface free energy 'non-stick' vessels are therefore not recommended for efficient processing.

While the end of mix point occurred at a similar time for the PMMA and titanium vessels, the time at after which the P1–P2 transition occurred (where the mixture reached its maximum temperature) was longer for the titanium vessel (36 ± 1 min) than the PMMA vessel (29 ± 1 min). Table 8 gives the results of the cooling rate analysis for the vessels. It can be seen that the Newtonian cooling constants were consistent between the PTFE, PMMA and insulated titanium vessels, suggesting similar thermal behaviour. However, since these values were taken when the mixer was turned off and the material cooling down, they may not provide the basis for a valid comparison when the material is mixing and heating up. Specifically, it is thought that the titanium was slowing the rate of heating by acting as a heat sink, particularly throughout the P1 stage where the thermal gradient across the vessels to ambient temperature was largest. This would be intuitive considering the markedly higher thermal effusivity, diffusivity, and conductivity of titanium in comparison to PMMA and PTFE [47]. The use of metallic vessels may however be useful when active heating or cooling is considered, since the vessel would be more thermally responsive. Other factors to be noted when considering vessel material may include electrical conductivity, density, mechanical strength, machinability, and cost.

3.7. Combined theory of movement modes

Based on literature observations, the experimental results, and conjecture, Fig. 7 gives a graphical indication of how the movement mode of the material likely depends on the wall slip and movement within the material, governed by the factors listed in Table 1.

Table 8
Cooling constants for each of the vessels when filled with 65 ml of the glass microbead formulation.

Vessel type	k (min^{-1})
Titanium Grade 5 (no insulation)	5.71×10^{-2}
Titanium Grade 5 (plastic base)	4.12×10^{-2}
PMMA	4.32×10^{-2}
PTFE	4.24×10^{-2}

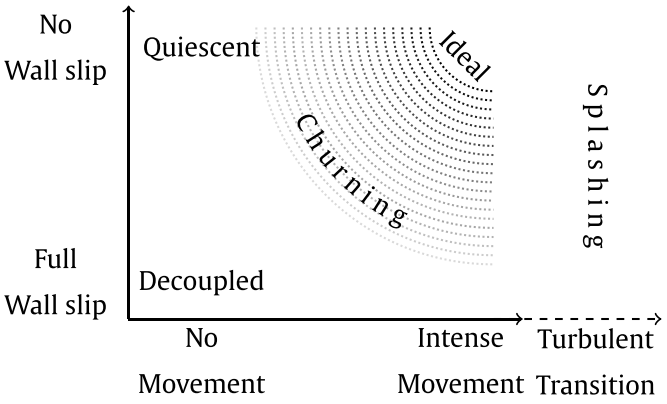

Fig. 7. Graphic of mixing mode dependence on wall slip and movement within the material. Darker shaded points indicate more vigorous churning, up to the ideal scenario.

If there is sufficient wall coupling and movement within the material (adequate Reynolds number), the movement mode will be churning. If wall slip is then reduced and/or there is more vigorous movement within the material (increased Reynolds number), churning will become more intense (ideal movement mode). Reducing the amount of movement by reducing the compliance (i.e. making the material harder to deform, reducing Reynolds number) will result in quiescence (no motion) if wall slip is negligible, or decoupled movement (bouncing as a cohesive lump) if there is sufficient slip. Reducing the amount of movement by reducing inertial forces would eventually result in quiescence. Though not a movement mode observed when mixing PBXs due to the high viscosities involved, also included for completeness is splashing [14], which will occur if material compliance or applied inertial forces are great enough for turbulent flow. By careful selection of the parameters shown in Table 1, the process engineer can therefore tailor the movement mode such that mixing efficiency is maximised.

4. Conclusions

The aim of this work was to assess the effects of acceleration (45 G, 50 G, and 55 G), vacuum application, and vessel material (PTFE, PMMA, and titanium) on RAM efficiency, as applied to an idealised PBX simulant. Also reported was consistency between mixer units (three LabRAMs). A method to determine the time and energy required for mixing completion was developed for this purpose. It was demonstrated that by interpreting the mixer 'intensity' profile, the changing rheology of the vessel contents can be monitored. It was found that the shape of the profile relies on rheological changes stemming from both changing homogeneity and changing temperature of the material. The sharp profile features associated with these changes provided well defined markers that allowed the mixing progression to be easily compared between mixes. Time requirement for mixing was repeatable within an average standard deviation of ±10% over all the mixing conditions investigated (17 mixes total).

For the first time, the effect of acceleration on mixing efficiency was quantitatively reported. Mixes performed at lower acceleration had longer mixing times and required more energy to mix. This was likely due to slower rate of energy transfer limiting temperature rise and thus viscosity reduction, which was exacerbated by greater thermal losses from the vessel over the longer mixing times.

Considerable variation in baseline mixer 'intensity' and mixing behaviour was apparent between different LabRAM units, and researchers are cautioned that calibration of units may be required to ensure reproducible PBX products.

It was also found that while reduced pressure is beneficial for churning, premature degassing of the binder should be avoided.

Avoiding the low surface free energy PTFE vessel was found to reduce mixing time and energy requirements, though additional data is required to confirm the significance of the observations. A greater work of adhesion, thus lower contact angle, between the material and vessel wall enhancing the 'no-slip' coupling condition is believed to be responsible. This supports the hypothesis that 'no-slip' conditions are important for mixing efficiency. The longer P1 stage duration for the titanium vessel is attributed to its significantly higher thermal conductivity in comparison to the polymeric vessels, slowing the rate of internal temperature rise thus viscosity reduction.

Overall, this work quantitatively reports on the most important factors that affect the efficiency of RAM, ultimately laying the groundwork for process intensification of PBX mixing in research and industrial manufacture.

CRediT authorship contribution statement

A.J. Claydon: Conceptualization, Methodology, Formal analysis, Investigation, Data curation, Writing – original draft, Visualization, Project administration. **A.N. Patil:** Conceptualization, Methodology, Formal analysis, Investigation, Writing – original draft. **S. Gaulter:** Supervision, Writing – review & editing. **G. Kister:** Supervision, Writing – review & editing. **P.P. Gill:** Supervision, Writing – review & editing, Project administration, Funding acquisition.

Declaration of competing interest

The authors declare that they have no known competing financial interests or personal relationships that could have appeared to influence the work reported in this paper.

Acknowledgements

This publication is primarily adapted from Chapters 1–5 of the lead author's PhD thesis [18], funded by Cranfield University, United Kingdom and MBDA Missile Systems, United Kingdom. Additional data (that concerning the effect of vacuum) has been included from the MSc thesis of A.N. Patil [21], funded by the Defence Research and Development Organisation (India). The authors would like to thank K. Norris and the Shrivenham workshop team for manufacturing the mixing vessels, and technicians P. Wilkinson and N. Darcy for their assistance during practical work. Our thanks also go to The Falcon Project Ltd. (particularly D. Jubb, D. Fossey, and A. Stocker) and BAE Systems Land (UK) (particularly A. Burn and R. Davey) for providing material support and advice, and to Defence Equipment & Support (UK MoD) for funding the procurement of the LabRAM at Cranfield University. The authors also thank A. Vandenberg and K. Wille of The University of Connecticut for supplying the data used to reproduce the graph shown in Fig. 1.

Table B.1
Time requirement for the M–P1 transition (end of mix point) and P1–P2 transition (time of maximum temperature). ±1 standard deviation stated.

Acceleration	Unit	Vessel	Time (min)	
			M–P1	P1–P2
45 G	'A'	PMMA	21.3 ± 1.5	36.0 ± 2.9
50 G	'A'	PMMA	16.7 ± 1.9	28.9 ± 1.0
55 G	'A'	PMMA	09.6 ± 0.5	17.7 ± 1.9
50 G	'A'	PMMA	16.7 ± 1.9	28.9 ± 1.0
50 G	'C'	PMMA	09.1 ± 2.0	13.9 ± 2.1
50 G	'A'	PTFE	20.1 ± 2.2	35.5 ± 0.3
50 G	'A'	PMMA	16.7 ± 1.9	28.9 ± 1.0
50 G	'A'	Titanium	16.8 ± 0.6	35.9 ± 0.6

Appendix A. Drop shape analysis methodology

Young–Laplace drop shape analysis (DataPhysics OCA 20) was used to characterise the DEHA/HTPB binder mixture using the pendant drop technique in air and water media. This gave values for total surface tension and interfacial tension with water, of which the polar and disperse components of surface tension are known [48]. The polar and disperse components of the surface tensions for the binder mixture were then related [33–35] by:

$$\sigma_{IFT} = \sigma_{SFT_B} + \sigma_{SFT_W} - 2\left(\sqrt{\sigma^d_{SFT_B}\sigma^d_{SFT_W}} + \sqrt{\sigma^p_{SFT_B}\sigma^p_{SFT_W}}\right) \quad (A.1)$$

where σ_{IFT} is the interfacial tension between the binder mixture and water, σ_{SFT_B} is the total surface tension of the binder mixture, σ_{SFT_W} is the total surface tension of water, $\sigma^d_{SFT_B}$ and $\sigma^p_{SFT_B}$ are the dispersive and polar components of the binder mixture surface tension, and $\sigma^d_{SFT_W}$ and $\sigma^p_{SFT_W}$ are the dispersive and polar components of water surface tension. All have units of mJ m^{-2}. The equation was solved by substituting $\sigma^p_{SFT_B}$ as $\sigma_{SFT_B} - \sigma^d_{SFT_B}$, and finding $\sigma^d_{SFT_B}$ iteratively.

Young–Laplace drop shape analysis (DataPhysics OCA 20) was used to characterise surface samples of each vessel material using the sessile drop technique (contact angle determination) with probe liquids deionised water, diiodomethane, and ethylene glycol (of which the polar and disperse components of surface tension are known [33,48,49]). The linear form ($y = mx + c$) of Eq. (4) substituted into Eq. (5) is given as:

$$\frac{1}{2}(1 + cos\theta)\frac{\sigma_{SFT}}{\sqrt{\sigma^d_{SFT}}} = \sqrt{\sigma^p_{SFE}}\sqrt{\frac{\sigma^p_{SFT}}{\sigma^d_{SFT}}} + \sqrt{\sigma^d_{SFE}} \quad (A.2)$$

where θ is the contact angle (degrees), σ_{SFT} is the total surface tension of the probe liquid (mJ m^{-2}), σ^d_{SFT} and σ^p_{SFT} are the dispersive and polar components of the surface tension respectively (mJ m^{-2}), σ_{SFE} is the total surface free energy of the surface (mJ m^{-2}), and σ^d_{SFE} and σ^p_{SFE} are the dispersive and polar components of the surface free energy respectively (mJ m^{-2}). By plotting y against x for each of the probe liquids in contact with a surface sample, the squares of the gradient and the intercept of the resulting line of best fit equated to the polar and dispersive components of the surface free energy of the sample respectively.

Appendix B. Full mixing data

See Tables B.1 and B.2.

Table B.2
Energy requirement for the M–P1 transition (end of mix point) and P1–P2 transition (time of maximum temperature). ±1 standard deviation stated.

Acceleration	Unit	Vessel	Energy (kJ)	
			M–P1	P1–P2
45 G	'A'	PMMA	12.7 ± 0.5	33.9 ± 2.1
50 G	'A'	PMMA	12.1 ± 0.7	32.6 ± 0.6
55 G	'A'	PMMA	09.0 ± 0.3	23.9 ± 2.1
50 G	'A'	PMMA	12.1 ± 0.7	32.6 ± 0.6
50 G	'C'	PMMA	N/A	N/A
50 G	'A'	PTFE	12.9 ± 0.6	37.7 ± 3.4
50 G	'A'	PMMA	12.1 ± 0.7	32.6 ± 0.6
50 G	'A'	Titanium	12.4 ± 0.3	45.0 ± 1.6

References

[1] D.B. Todd, Mixing of highly viscous fluids, polymers, and pastes, in: Handbook Of Industrial Mixing: Science And Practice, John Wiley & Sons, Inc., 2004, pp. 987–1025, http://dx.doi.org/10.1002/0471451452.ch16.

[2] A.C. Hordijk, A.E.D.M. van der Heijden, Mixing, in: Energetic materials; particle processing and characterization, Wiley-VCH Verlag GmbH, ISBN: 9783527302406, 2005, pp. 225–236.

[3] Charles Ross & Son Company, High viscosity mixer designs and applications, 2021, https://www.mixers.com/whitepapers/hvm_designs_whitepaper.pdf (Accessed 09 Jun 2021).

[4] Charles Ross & Son Company, How to choose the right mixer for high-viscosity mixing applications, 2021, https://www.mixers.com/whitepapers/high%20viscosity%20mixing.pdf (Accessed 09 Jun 2021).

[5] D.A. Dahlstrom, R.C. Bennett, R.G. Emmet, P. Harriott, T. Laros, W. Leung, S. Miller, B. Morey, J. Oldshue, G. Priday, C. Silverblatt, J. Slottee, J. Smith, Liquid-solid operations and equipment, in: Perry's Chemical Engineers' Handbook, Seventh Ed., McGraw-Hill Pub., ISBN: 9780071154482, 1997, pp. 25–29.

[6] R.J. Davey, J.M. Wilgeroth, A.O. Burn, Processing Studies of Energetic Materials using Resonant Acoustic Mixing Technology, BAE Systems Land (UK), Glascoed, Usk, UK, 2019.

[7] M. Andrews, C. Collet, A. Wolff, C. Hollands, ResonantAcosutic Mixing processing and safety, Propellants Explos. Pyrotech. 45 (2019) 77–86, http://dx.doi.org/10.1002/prep.201900280.

[8] Resodyn Acoustic Mixers, Inc., How RAM mixes, 2021, https://resodynmixers.com/how-ram-mixes/ (Accessed 31 Dec 2021).

[9] Resodyn Acoustic Mixers, Inc., How RAM mixes, 2021, https://resodynmixers.com/applications/viscous/ (Accessed 31 Dec 2021).

[10] M.D. McPherson, Propellant and explosives production method by use of resonant acoustic mix process, Patent WO 2009/091430 A1.

[11] P.A. Lucon, G. Sperry, J. Whaley, RAM Mixing of Liquids and Pastes, Butte, MT, USA, Resodyn Technical Interchange, 2016.

[12] D. Nance, Simulating the Resonant Acoustic Mixer, Air Force Research Laboratory, Elgin, FL, USA, 2013, AFRL-RW-EG-TR-2013-079.

[13] D. Nance, An examination of the resonant acoustic mixer's flow field, Air Force Research Laboratory, Elgin, FL, USA, 2013, AFRL-RW-EG-TR-2013-108.

[14] P.A. Lucon, J. Whaley, Liquids and Pastes Mixing Regimes, Resodyn Technical Interchange, Butte, MT, USA, 2016.

[15] J. Hilden, M. Sullivan, M. Polizzi, J. Wade, J. Greer, M. Keeney, Power consumption during oscillatory mixing of pharmaceutical powders, Powder Technol. 338 (2018) 44–54, http://dx.doi.org/10.1016/j.powtec.2018.06.004.

[16] E.L. McCloy, P. Wilkinson, P.P. Gill, Resonant Acoustic Mixing: Pushing The Boundaries, Cranfield University, 2016.

[17] P.A. Lucon, Mixing with Vacuum Assist, Resodyn Technical Interchange, Butte, MT, USA, 2016.

[18] A.J. Claydon, Resonant Acoustic Mixing of Polymer Bonded Explosives, (PhD thesis), Cranfield University, 2020, http://dspace.lib.cranfield.ac.uk/handle/1826/16337.

[19] A. Vandenberg, K. Wille, Evaluation of resonance acoustic mixing technology using ultra high performance concrete, Constr. Build. Mater. 164 (2018) 716–730, http://dx.doi.org/10.1016/j.conbuildmat.2017.12.217.

[20] S.L. Coguill, Z.R. Martineau, Vessel Geometry and Fluid Properties Influencing Mix Behavior of Resonant Acoustic Mixing, 38th International Pyrotechnics Seminar, Denver, CO, USA, 2012, http://dx.doi.org/10.13140/2.1.2920.8646.

[21] A.N. Patil, P.P. Gill, Resonant Acoustic Mixing – The Future of Propellant Manufacturing, Cranfield University, 2018.

[22] T.G. Yew, P.P. Gill, P. Wilkinson, Process Parameters for Resonant Acoustic Mixers (RAM), Cranfield University, 2015.

[23] J.T. Miller, D.A. Bode, S.L. Coguill, ResonantAcoustic mixing; design and process considerations concerning vessel/case geometry and mix versus cure time when preparing composite solid propellant, JANNAF 36th Propellant and Explosives Development and Characterization Joint Subcommittee Meeting, Orlando, FL, USA, 2010, http://dx.doi.org/10.13140/2.1.1872.2881.

[24] E.R. Beckel, K.E. Lee, J.C. Marin, A.H. Shah, Processing of Explosives at ARDEC Using the LabRAM, U.S. Army Armament Research, Development and Engineering Center, 2016.

[25] J.G. Osorio, K. Sowrirajan, F.J. Muzzio, Effect of resonant acoustic mixing on pharmaceutical powder blends, Adv. Powder Technol. 27 (2016) 1141–1148, http://dx.doi.org/10.1016/j.apt.2016.03.025.

[26] R.A. Layton, W.R. Murray, J.L. Garbini, The control of power for efficient batch mixing, Propellants Explos. Pyrotech. 22 (1997) 269–278, http://dx.doi.org/10.1002/prep.19970220505.

[27] D. Jubb, Private Communication, The Falcon Project Ltd., 2019.

[28] Resodyn Acoustic Mixers, Inc., Products, 2021, https://resodynmixers.com/products/ (Accessed 31 Dec 2021).

[29] J. Whaley, Private Communication, Resodyn Acoustic Mixers, Inc., 2019.

[30] M. Lewin, A. Mey-Marom, R. Frank, Surface free energies of polymeric materials, additives and minerals, Polym. Adv. Technol. 16 (2005) 429–441, http://dx.doi.org/10.1002/pat.605.

[31] M. Mantel, J.P. Wightman, Influence of the surface chemistry on the wettability of stainless steel, Surf. Interface Anal. 21 (1994) 595–605, http://dx.doi.org/10.1002/sia.740210902.

[32] J.E. Castle, The composition of metal surfaces after atmospheric exposure: An historical perspective, J. Adhes. 84 (2008) 368–388, http://dx.doi.org/10.1080/00218460802004477.

[33] D.K. Owens, R.C. Wendt, Estimation of the surface free energy of polymers, J. App. Polym. Sci. 13 (1969) 1741–1747, http://dx.doi.org/10.1002/app.1969.070130815.

[34] D.H. Kaelble, Dispersion-polar surface tension properties of organic solids, J. Adhes. 2 (1970) 66–81, http://dx.doi.org/10.1080/0021846708544582.

[35] W. Rabel, Einige Aspekte der Benetzungstheorie und ihre Anwendung auf die Untersuchung und Veränderung der Oberflächeneigenschaften von Polymeren, Farbe Und Lack 77 (1971) 997–1005.

[36] M.E. Schrader, Young–Dupré revisited, Langmuir 11 (1995) 3585–3589, http://dx.doi.org/10.1021/la00009a049.

[37] M. Cloitre, R.T. Bonnecaze, A review on wall slip in high solid dispersions, Rheol Acta 56 (2017) 283–305, http://dx.doi.org/10.1007/s00397-017-1002-7.

[38] H. Howe, J. Warriner, A. Cook, S. Coguill, L. Farrar, Apparatus and Method for Resonant Vibratory Mixing, Patent US 7188993 B1.

[39] H. Howe, J. Warriner, A. Cook, S. Coguill, L. Farrar, Method for Resonant Vibratory Mixing, Patent US 7866878 B2.

[40] P.A. Lucon, RAM Power Considerations, Resodyn Technical Interchange, Butte, MT, USA, 2016.

[41] J.T. Miller, A. Luebbering, S. Coguill, P. Lucon, Mix power, 2013, Resodyn Forum: Industrial Outcomes in ResonantAcoustic Mixing, Butte, MT, USA.

[42] J.G. Osorio, F.J. Muzzio, Evaluation of resonant acoustic mixing performance, Powder Technol. 278 (2015) 46–56, http://dx.doi.org/10.1016/j.powtec.2015.02.033.

[43] R.F. Du Plessis, Private Communication, Roxel (UK Rocket Motors) Ltd., 2019.

[44] L. Haichuan, X. Chengbin, G. Yonghui, L. Lirong, Z. Haijin, Cement slurries with rheological properties unaffected by temperature, SPE Drill. & Compl. 30 (2016) 316–321, http://dx.doi.org/10.2118/178922-PA.

[45] NATO, Explosives, specification for RDX (Hexogene), STANAG-4022.

[46] S. Wu, Calculation of interfacial tension in polymer systems, J. Polym. Sci. C 34 (1971) 19–30, http://dx.doi.org/10.1002/polc.5070340105.

[47] Thermtest instruments materials properties database, 2021, https://thermtest.com/materials-database (Accessed 09 Jun 2021).

[48] K.F. Gebhardt, Grundlagen der physikalischen Chemie von Grenzflächen und Methoden zur Bestimmung grenzflächenenergetischer Größen, FhG IGB Stuttgart, 1982.

[49] H.J. Busscher, A.W.J. van Pelt, P. de Boer, H.P. de Jong, J. Arends, The effect of surface roughening of polymers on measured contact angles of liquids, Colloids Surf. 9 (1984) 319–331, http://dx.doi.org/10.1016/0166-6622(84)80175-4.